ADVANCED NONEQUILIBRIUM MODELLING OF DC TUNGSTEN-INERT GAS ARCS

M. Baeva*, D. Uhrlandt

Leibniz Institute for Plasma Science and Technology, Felix-Hausdorff-Strasse 2, 17489 Greifswald, Germany

* baeva@inp-greifswald.de

Abstract. The paper is concerned with the state-of-the-art nonequilibrium modelling of a DC tungsten-inert gas arc plasma. The advanced description involves the two-way interaction between the plasma and the electrodes. Results in atmospheric pressure argon demonstrating important features of the arc plasma are presented and discussed. First results in the presence of metal vapour released from the molten anode are presented. Outlook for further developments in nonequilibrium arc modelling are discussed.

Keywords: nonequilibrium, arc plasma, magnetohydrodynamic model, diffusion, plasma-electrode interaction.

1. Introduction

Significant progress has been continuously achieved in arc plasma modelling [1]. The unified description of the arc plasma and the electrodes has been an important step in the improvement of the boundary conditions of the plasma solution [2–4]. New models have been developed for atmospheric pressure DC arcs in argon with the simplified configuration of a tungsten-inert gas (TIG) arc. The latter includes a doped tungsten cathode with a conical tip and a flat anode made of copper or steel. The models usually consider axial symmetry and stationary conditions, and neglect metal evaporation. The state-of-the art models are aimed at improving the description in the regions with deviations from local thermodynamic equilibrium (LTE), i.e. the near-electrode regions and the arc fringes. The near-electrode regions are responsible for the arc attachment and the current transfer. The processes in the arc fringes have a strong influence on the arc shape. The models have to be capable of predicting many arc properties: distributions of electric current density and potential, temperatures of electrons and heavy particles, the arc voltage including contributions of the arc column and the near-electrode regions, and the heat loads on the electrodes.

Models solving the nonequilibrium near-electrode regions respectively on the cathode side [5] and on the anode side [6] and applying LTE conditions on the boundary between the equilibrium arc column and the nonequilibrium boundary layer have been developed. They are one-dimensional due to the big computational effort and do not cover the entire arc body because of the high degree of quasi-neutrality in the arc column. Mostly two- but also three-dimensional models of the near-cathode region have been published (see e.g. [7–9]), which apply the concept of a sub-division of the near-electrode regions into a space-charge sheath, a Knudsen layer, an ionization layer, and a layer of thermal nonequilibrium in the direction

away from the electrode, and the model proposed by Benilov and Marotta [10]. Such models have been further adopted for a coupling to a model of the arc column. Approaches to arc plasma modelling, which take into account the properties of the near-electrode regions, have been developed so far. Their variety can be divided into three main groups. In the models of the first group, the LTE description of the arc column is combined with a nonequilibrium description of the near-cathode region including all sub-regions (see e.g. [11–14]). These models improve, in general, the arc plasma description since they take into account the contribution of the cathode boundary layer. However, the LTE description of the arc column neglects the electrical conductivity in the arc fringes and necessarily overestimates the current density, the plasma temperature, and the voltage drop in the arc column (see [15] and the references therein). The models of the second group employ ionization equilibrium and thermal nonequilibrium in the description of the arc plasma column. Therefore, the arc plasma column is characterized by two temperatures respectively associated with the electrons and the heavy particles of the plasma. The nonequilibrium boundary layer is described similarly to the models in the first group except that the layer of thermal relaxation is not necessarily required. The cathode boundary layer described according to [10] and coupled to a two-temperature arc plasma within the transfer function concept has been applied in [16]. Further developments have led to the model of nonlinear surface heating [7] which provided boundary conditions for the two-temperature arc plasma model [17], i.e. the cathode boundary layer is assumed independent of the plasma column. The models of the third group provide a fully nonequilibrium description of the arc plasma avoiding the assumptions of both thermal and ionization equilibria (see e.g. [18] and the most recent development [19]). If quasi-neutrality is assumed, the description of the arc

plasma column is naturally extended to include the ionization layer. Hence, a description of the boundary layers is related only to the space-charge sheaths adjacent to the electrodes. The Knudsen layer, in which the transition from the ionization layer to the space-charge sheath occurs, is taken into account in the boundary conditions of the hydrodynamic description of the arc column. The models of the third group representing the most advanced modelling of TIG arcs up to date are considered in the present work.

2. General and advanced features of the arc model

An almost complete description of the modelling approach is given in a previous publication [19]. In what follows, a summary will be given outlining its main features and new developments. The modelling approach couples a magneto-hydrodynamic (MHD) simulation of the arc, a description of the arc-electrode interaction, and the heat and current balances of the electrodes. The MHD arc simulation is based on the Navier-Stokes equation system for conservation of mass, momentum, energy, and species. It is coupled with the Maxwell equations, Ohm law and the equation of state. The arc plasma is considered as quasi-neutral and contains electrons, atoms and singly charged ions of argon. Assumptions of thermal and ionization equilibrium are avoided. The MHD approach is valid not only in the arc column but also in the pre-sheath regions of the electrodes and in the arc fringes. Separate energy equations are solved for electrons and heavy particles, which account for a convective transport, the energy flux due to thermal conduction, transport of enthalpy due to diffusive fluxes and thermal diffusion, and gain and loss of energy due to Joule heating, elastic and inelastic collisions, and radiation. Assuming a Maxwellian energy distribution, the electrons are characterized by a temperature T_e while the the atoms and ions are characterized by a common temperature T. A general species equation is solved for the ions, which accounts for the transport processes of convection and diffusion as well as the production and loss due to ionization and recombination. The mass fluxes of the plasma species are expressed in terms of multicomponent diffusion based on the Stefan-Maxwell equations and the effective binary approach [20, 21]. These fluxes contain driving forces resulting from gradients in mass fractions, temperatures and pressure, and drift of charged particles in the electric field. Hence, the electric current density consists of a diffusive component and a drift component and represents the generalized formulation of the Ohm law. The atom density is determined with the equation of state and the Dalton law. The Lorenz force is considered in the momentum conservation equation to take into account the pressure gradient produced by the self-induced magnetic field. New developments of the nonequilibrium model reported in [19] are concerned with a more general representation of the terms caused by thermal diffusion and the transport parameters of the plasma. The latter are calculated in terms of the Chapman-Enskog theory with high order of approximation [22] and allow us an extended description in cases when metal vapour is released from the molten anode. Current and heat conduction are considered in the electrodes with temperature dependent thermal and electrical conductivity of the material. The quasi-neutral plasma and the electrodes are coupled through the tiny regions of the space-charge sheaths (with a thickness of the order of the Debye length) which are treated as dimensionless. The transition from the pre-sheath (included in the description of the arc column) to the space-charge sheath occurs in the Knudsen Layer (with a thickness of the order of the mean free-path of ion-neutral collisions) where the ions are accelerated up to the Bohm speed. The properties of this layer are accounted for in the boundary conditions of the hydrodynamic description [23]. The two-way interaction between the arc plasma and the electrodes is based on the balance of the electron energy and the total energy in the space-charge sheath as formulated in [23]. Contributions of ions and electrons from the plasma and electrons emitted from the metal electrode are taken into account for the continuity of the normal current density and the energy balance. The heat exchange with the electrodes includes the power deposited in the sheath and the cooling due to the transit of electrons from the metal into the plasma, the power released at the surface due to ion recombination, and black body radiation. The two-dimensional distribution of the normal current density and the voltage drop in space-charge sheath, and the arc voltage are obtained self-consistently for a given total arc current.

The modelling approach is applied to study TIG arcs in argon at atmospheric pressure. The schematic of the general arrangement is shown in figure 1 to the half of the arc geometry since axial symmetry is assumed. The cathode is a cylindrical rod made of ceriated tungsten (WC20) with a radius of 2 mm and various shapes of the tip. The anode is a plate made of steel or copper and is perpendicular to the arc axis. The inter-electrode distance d_{ca} is changed from 5 mm up to 120 mm to simulate cases of interest. Hence, the same physical model is used to study the arc column and the near-electrode regions for various arc lengths and operating conditions. The model is realized on the computational platform COMSOL Multyphysics [24] which is based on the Finite Element Method (FEM) with a computational domain of 5×10^4–9×10^4 mesh elements. Appropriate boundary conditions completing the model are presented in [19, 23]. All dependent variables have zero gradients on the axis of symmetry. The temperature of heavy particles approaches the surface temperature of the walls. The temperature of the gas inflow and nozzle/constrictor tube walls is set to 300 K and that at the base of the cathode is 500 K. At the bottom of the anode, the temperature
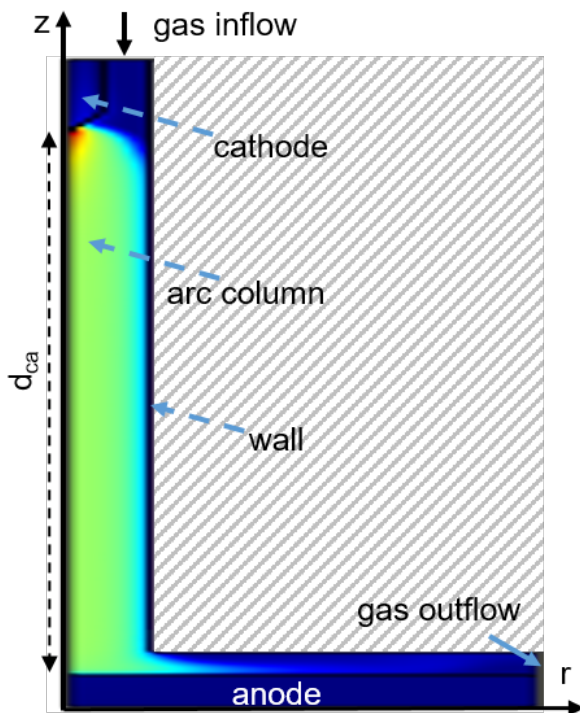
Figure 1. The general schematic view of the arc arrangement.

is set to 300 K to simulate a water cooling or a heat flux coefficient of $50\,\mathrm{Wm^{-2}K^{-1}}$ for an unforced air cooling is set. The outer boundaries are electrically and magnetically insulated except the cathode base and the anode bottom on which electric potential is specified (the anode is grounded).

3. Results and discussion

The results presented in this section are obtained under specific requirements depending on the focus of interest. Therefore, some deviation from the general conditions mentioned above can occur. These deviations are specified with the corresponding case of investigation - effects related to the cathode shape, the arc length, the processes in the anode region, and the presence of metal vapours in the arc plasma.

3.1. Effects of the cathode tip shape

The arc plasma parameters depend among others on the geometry of the cathode. Measurements of the plasma temperature concerned with the cathode shape have been reported by Haidar and Farmer [25], who have studied the plasma temperature (LTE conditions assumed) near the conical shaped cathode tip and the cathode surface temperature for cone angles from 12° to 150°. In these experiments, the dc arc was operated in argon at atmospheric pressure between a cathode made of thoriated tungsten and a copper plate (both electrodes were water-cooled). The measurements showed for all angles a maximum of the plasma temperature near the cathode tip. The plasma

temperature was largest for a cone angle of 60°. The results were qualitatively explained by the interplay between the heat mechanisms of conduction, convection and radiation, and the thermionic cooling of the cathode. However, no modelling has been carried out to provide a detailed analysis.

We applied the advanced nonequilibrium model of TIG arcs for several shapes of the cathode tip, these are a cone with an angle of 30° and 60°, a hemisphere, and a flat truncation of the cylindrical rod. The conical tips are considered with a plateau radius of 0.2 mm and a fillet on the edge with a radius of curvature of 0.1 mm. The inter-electrode distance is $d_{\mathrm{ca}} = 5\,\mathrm{mm}$, the arc current is 200 A, and the flow rate is 15 slpm. The stick-off distance, i.e. the axial distance between the cathode tip and the end of the nozzle wall, is 4.5 mm.

Figures 2 and 3 show the radial profiles of the temperatures of electrons and heavy particles along a line-out at axial distance from the cathode tip of respectively 1 mm and 3 mm. For all shapes of the cathode tip, the arc plasma is in thermal equilibrium for radial positions up to approximately 2.5 mm (Fig. 2) and 4 mm (Fig. 3). Closer to the cathode tip, the common temperature is largest for a cone angle of 60° and smallest for the flat tip of the cathode with a maximum difference of about 10000 K. The variation of the plasma temperature becomes smaller as the axial distance from the cathode tip increases (Fig. 3). At an axial distance of 3 mm, the temperature variation with the cone angle is insignificant. This trend appears in the radial profiles of the magnitude of the current density (Fig. 4) so that closer to the cathode tip the current density is a bit higher for a cone angle of 60° in comparison to that for 30° and for the rounded tip compared to the flat one. Moving towards the anode, the variation in the radial profiles for the conical tips, on the one hand, and for the rounded and the flat tip, on the other hand, becomes very small.

The modelling results confirm the experimental findings by Haidar and Farmer [25] concerning the higher plasma temperature near the tip for a cone angle of 60° than for 30°. In order to analyse the results, we consider the conditions on the cathode surface, in the cathode bulk, and close the cathode tip in the plasma. Figure 5 shows the distributions of the temperature (lines with solid symbols) and the normal current density (lines with open symbols) on the cathode surface as a function of the distance measured from the centre of the cathode tip along the cathode surface. The distance of 0.2 mm corresponds to the radius of the plateau, which edge is rounded and forms the cathode tip. The conical part of the cathode differs in its length for both cone angles. Although the tip ends are of equal area, the normal current density and the surface temperature are slightly higher for a cone angle of 30°. The current density and Ohmic heating in the cathode bulk are presented respectively by means of arrow indicators and iso-lines with la-
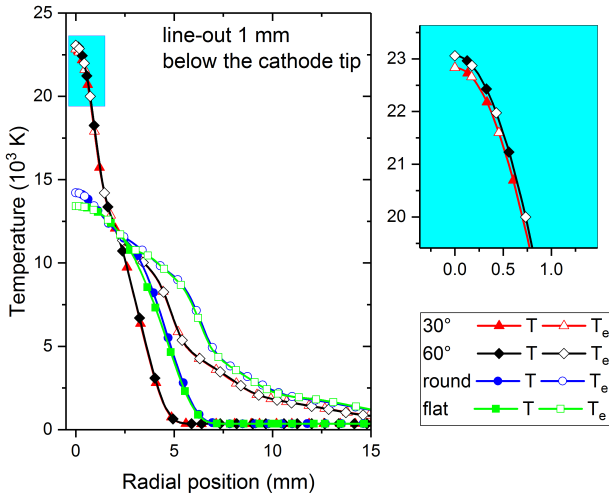
Figure 2. Radial profiles of the temperatures of electrons (lines with open symbols) and heavy particles (lines with solid symbols) for various shapes of the cathode tip along a line-out with an axial distance from the cathode tip of 1 mm.
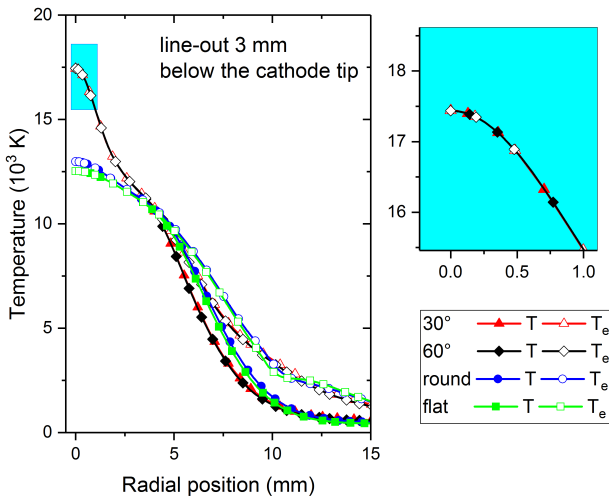

Figure 3. Radial profiles of the temperatures of electrons (lines with open symbols) and heavy particles (lines with solid symbols) for various shapes of the cathode tip along a line-out with an axial distance from the cathode tip of 3 mm.
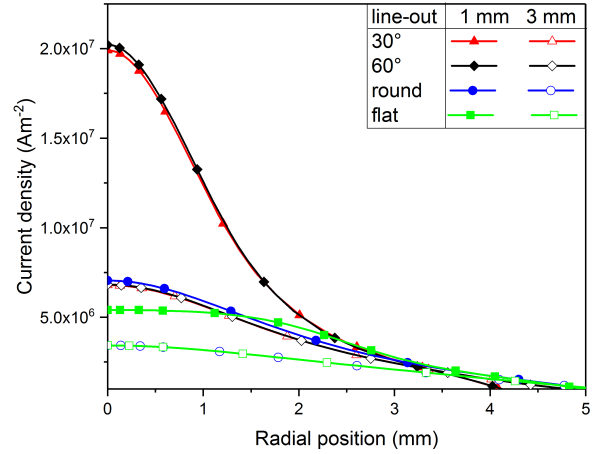

Figure 4. Radial profiles of the magnitude of the current density for various shapes of the cathode tip along a line-out with an axial distance from the cathode tip of 1 mm (lines with solid symbols) and 3 mm (lines with open symbols).
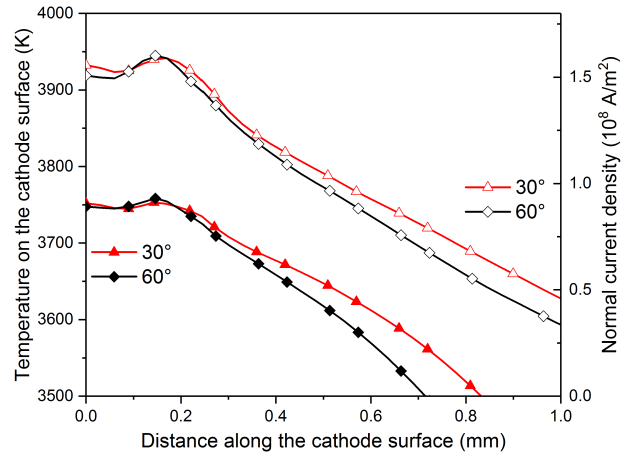

Figure 5. The temperature (solid symbols) and the normal current density (open symbols) on the cathode surface for a cone angle of 30° (triangles) and 60° (diamonds). The distance is measured from the centre of the cathode tip.

bels in units of $10^{10}\,\mathrm{W/m^3}$ in Figure 6. The current density and the ohmic heating are higher in the cathode bulk for a cone angle of 30° due to the smaller cross-section area. Well pronounced maxima near the inclined side of the cathode can be seen in both cases though at different axial positions. The higher current density and ohmic heating in the cathode bulk for the 30°-conical tip lead to the higher temperature of the cathode. However, in the plasma region close to the cathode tip, the conditions change(Figures 2 and 4). Figure 7 shows the terms of the conservation equation of electron energy (see e.g. Eq. (3) [28]) along a radial line-out with an axial distance from the cathode tip of 1 mm. The equation can be written into the form

$$\nabla \cdot \left(\frac{5}{2}n_\mathrm{e}k_\mathrm{B}T_\mathrm{e}\mathbf{u}\right) + \nabla \cdot \mathbf{J}_\varepsilon + \frac{e}{m_\mathrm{e}}\mathbf{J}_\mathrm{e} \cdot \mathbf{E}$$
$$+Q_{e-n}^{\mathrm{el}} + Q_{e-h}^{\mathrm{in}} + Q_{\mathrm{rad}} = 0. \tag{1}$$

In Equation (1), n_e, T_e, e and m_e denote respectively the number density, the temperature, the electric charge and the mass of electrons, $\mathbf{J}_\varepsilon$ is the density of the electron energy flux, $\mathbf{J}_\mathrm{e}$ is the mass flux of electrons, and $\mathbf{E}$ is the electric field. k_B is the Botzmann constant. The first term in Equation (1) describing the change of electron energy change due to the enthalpy flux is denoted in Figure 7 as Q_{conv}. The second term represents the divergence of the density of the electron energy flux ($Q_{\mathrm{div}J_\varepsilon}$ in Figure 7). The third term is the ohmic heating of the electrons by the electric field (Q_{ohm}). The last three terms represent respectively
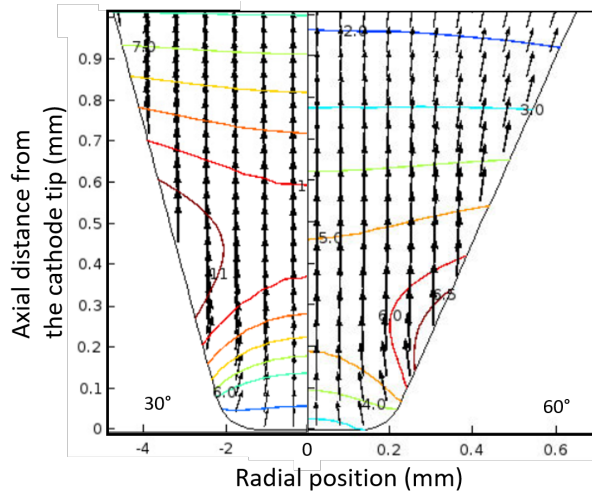
Figure 6. The current density (arrow indicators) and ohmic heating in units of 10^{10} W/m^3 (iso-lines) in the conical part of the cathode for cone angles of 30° and 60°.
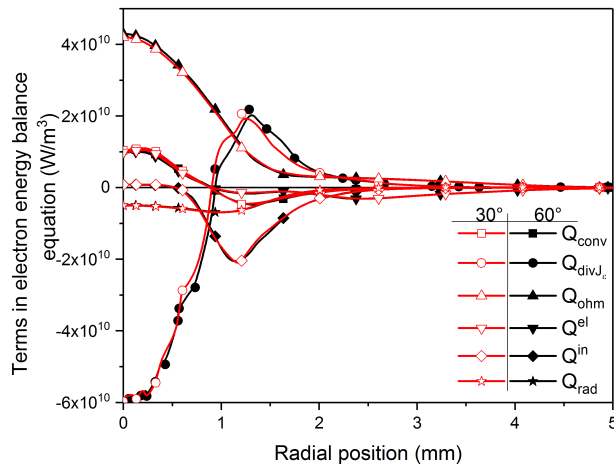

Figure 7. Terms of the electron energy balance for a cone angle of 30° (open symbols) and 60° (solid symbols) along a radial line-out in axial distance from the cathode tip 1 mm.

the energy change due to elastic (Q^{el}) and inelastic collisions (Q^{in}) between electrons and heavy particles, and radiation (Q_{rad}). In general, the results show very similar behaviour and values of the terms for both cone angles. Close to the axis, where small differences in the current density and temperature occur (Figures 2 and 4), the value of Q_{ohm} is slightly higher for the 60°-cathode. Q_{divJ_ε} is the dominant term in Equation (1) and it ensures the energy balance by the transport of a local energy excess. The physical picture is very complex because of the and non-linear nature of the problem and the explanation of the temperature maximum for a cone angle of 60° seems to be much more sophisticated than the considerations suggested in [25]. A plausible explanation is provided by the two-directional plasma-electrode interaction. The detailed analysis of the heat load to the conical
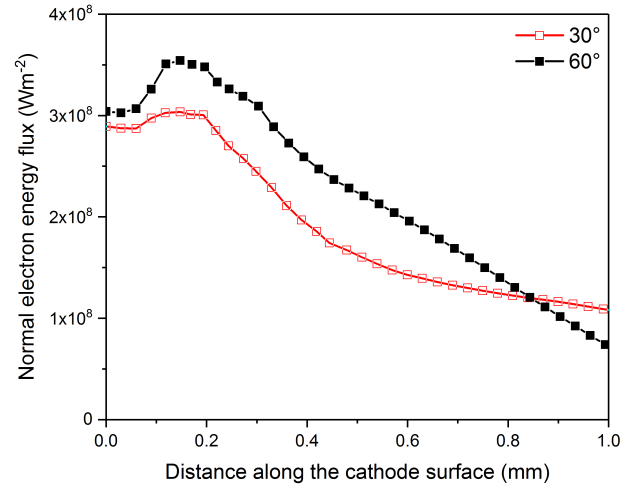

Figure 8. Normal component of the density of electron energy flux at the cathode for cone angles of 30° (open symbols) and 60° (solid symbols)

cathode of TIG arcs presented in [28] (see Figure 10 and Equation (29) therein) shows that a huge amount of the electric power is transferred from the space-charge sheath to the plasma electrons. This energy amount is less for a cone angle of 30° as the results in Figure 8 show.

3.2. Effects due to arc length variation

A variation of the arc length (the inter-electrode distance) touches on various important issues, e.g. industrial applications, plasma diagnostics, theoretical description and modelling of arc plasmas. Arc length variations occur in configurations with moving electrodes and in experiments concerned with the determination of the electric field strength among others. We consider in this part the impact of the arc length on the arc plasma.

Figure 9 presents the arc voltage as a function of the inter-electrode distance for an arc current of 100 A. The results are obtained with the nonequilibrium model and from experiments [26], in which the anode is a water cooled copper plate and the cathode has a conical tip of 60° and is made of ceriated tungsten (WC20). The slope of the nearly linear dependence of the arc voltage on the arc length at inter-electrode distances larger than 3 mm is used to estimate an average electric field of about 400 V/m. The non-linearity becomes stronger for distances below 3 mm. The extrapolation of this dependence to zero arc length provides the sum of the voltage drops in the space-charge sheaths, the cathode, and the anode. In this sum of about 8 V, the biggest contribution is assigned to the average voltage drop in the cathode space-charge sheath.

The two-dimensional distribution of the electron density for arc lengths of 2, 6 and 10 mm is shown in Figure 9. It indicates that a decrease of the arc length from 10 mm to 6 mm is related to a shortening of the plasma column in front of the anode. The region in
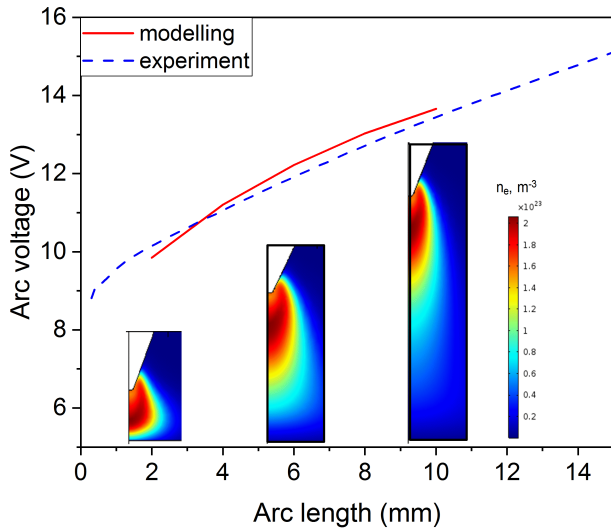
Figure 9. The arc voltage as a function of the arc length at arc current of 100 A. The two-dimensional distributions of the electron density for arc lengths of 2, 6, and 10 mm are shown to illustrate the arc structure.
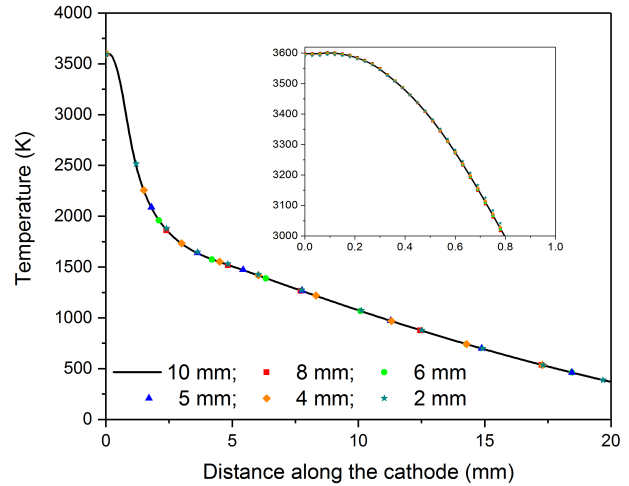

Figure 10. The temperature on the cathode surface as a function of the distance along the cathode. The distance is measured from the tip centre. The solid line presents the results for an arc length of 10 mm. Symbols present the results for shorter arc lengths.
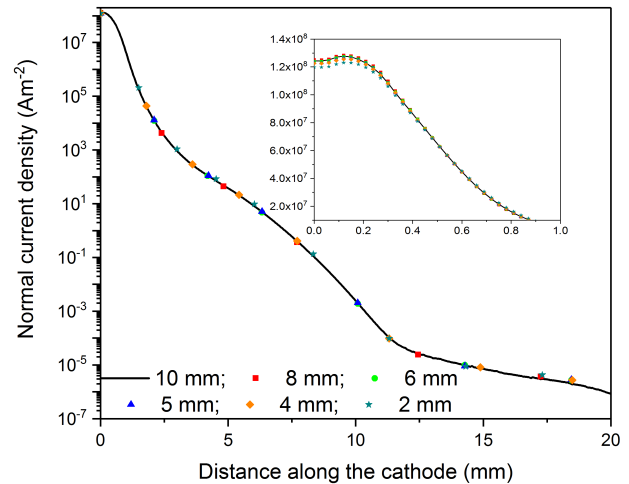

Figure 11. The normal current density on the cathode surface as a function of the distance along the cathode. The distance is measured from the tip centre. The notations are the same as in Fig. 10.

front of the cathode tip almost does not change. This effect results in the nearly linear dependence of the arc voltage on the arc length. The further decrease of the arc length, however, causes modifications in the arc structure. The hot arc core tends to occupy a great part of the inter-electrode gap and expands radially. As a result, the arc voltage decreases non-linearly with the arc length.

Figures 10, 11, and 12 present respectively the temperature on the cathode surface, the normal current density and the voltage drop in the cathode space-charge sheath for various arc lengths and an arc current of 100 A. The results obtained show a weak dependence on the arc length, i.e. the conditions in the cathode boundary layer are weakly affected by the rest of the arc. The temperature of the cathode, the normal current density, and the voltage drop decrease in the central part of the cathode tip for shorter arc lengths (see also the enlarged view of this area). The temperature and the normal current density slightly increase towards the end of the cathode for shorter arc lengths whereas the voltage drop in the space-charge sheath is consistently lower along the entire distance for shorter arc lengths. Moreover, the difference becomes much more pronounced. At distances beyond about 11.5 mm, the ion component of the normal current density exceeds the emission current component. Towards the end of the cathode, the ion current component is the dominant one. The voltage drop in the space-charge sheath is strong enough to suppress electrons diffusing from the plasma.

Models describing the cathode boundary layer, which includes the ionization layer and the space-charge sheath, are based on the assumption that the plasma-cathode interaction is independent of processes in the arc column [10, 27]. The weak dependence of the

temperature and the normal current density on the arc length are likely to confirm this assumption. A detailed comparison of results for TIG arcs obtained by the advanced nonequilibrium model [19] and a model of the cathode boundary layer [7] shows a qualitative agreement in the behaviour of the temperature and the normal current density on the cathode surface [28]. Nevertheless, they differ since the plasma parameters obtained by means of the nonequilibrium model certainly differ from the integral values evaluated only in the cathode boundary layer.

3.3. Effects in the anode region

In this part, we discuss the influence of the conditions in the region between the tube end (1) and the anode surface on the arc attachment on the anode. The region has an axial length of 10 mm. Fig. 13 shows
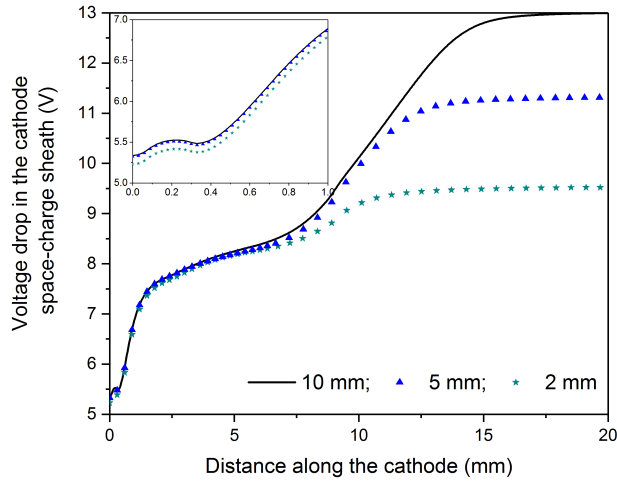
Figure 12. The voltage drop in the cathode space-charge sheath as a function of the distance along the cathode for arc lengths of 10 mm (solid line), 5 mm (triangles), and 2 mm (stars). The distance is measured from the tip centre.

Figure 13. Iso-lines of temperatures in kelvin of heavy particles (black) and electrons (coloured) and normalized arrow indicators of the gas flow in the anode region of the arc at a gas flow rate of 4.5 slpm and an arc current of 200 A.

Figure 14. Iso-lines of temperatures in kelvin of heavy particles (black) and electrons (coloured) and normalized arrow indicators of the gas flow in the anode region of the arc at a gas flow rate of 1.3 slpm and an arc current of 200 A.

the two-dimensional distribution of the electron and heavy particle temperatures, and the flow direction obtained for an arc current of 200 A and a gas flow rate of 4.5 slpm. The hot arc region which is enclosed by the iso-line of 11000 K is in thermal equilibrium ($T = T_e$). A departure from thermal equilibrium occurs for temperatures below 10000 K. The hot gas flow impinging on the anode surface is directed towards the open boundary. A cold gas flow enters the upper patch of the open boundary and moves along the bottom tube edge towards the arc. The cathode jet dominates the arc and leads to the bell-shape formation which is typical for the diffuse arc attachment on the anode [29]. A completely different situation appears after reducing the gas flow rate to 1.3 slpm (Fig. 14). The hot arc region is significantly shorted, an anode jet is built and collides with the cathode jet approximately 1.5 mm below the tube edge. The hot gas flows along the bottom tube edge towards the open boundary, while the cold gas flows towards the arc. This causes a contraction of the bottom part of the arc so that the arc attachment on the anode becomes constricted. The results confirm the experimental findings in [30] and the modelling predictions in [31]. The role of macroscopic flows for the formation of a constricted arc attachment has been underlined in the overview of the processes and conditions in the anode region given in [29]. Not only the extension of the region of thermal nonequilibrium but also different behaviour related to the ionization nonequilibrium have been recently predicted [32]. In the diffuse mode, the nonequilibrium electron density exceeds the equilibrium value over the entire length of the anode region. In the constricted mode, this behaviour is observed till the stagnation position. Beyond this position, the nonequilibrium electron density is lower than the equilibrium one. Fig. 15 presents the axial flow velocity and the modulus
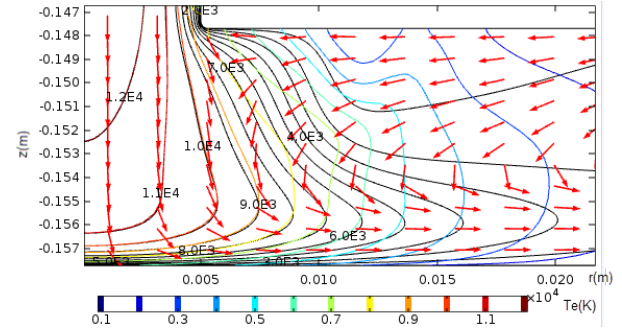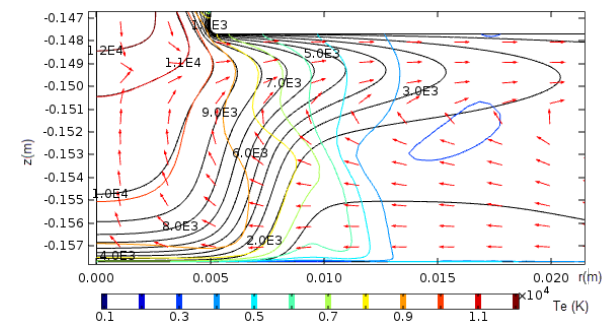
of the axial electric field $|E_z|$ over the distance to the anode. The regions of respectively the cathode and the anode jets are indicated. At the position of stagnation, $|E_z|$ exhibits a local minimum in the constricted arc. In the vicinity of the anode, the electric field in both modes undergoes a field reversal (corresponding to a negative anode fall in the electric potential). However, the position of the field reversal is closer to the anode and the potential drop amounts approximately 1 V in the constricted mode. In the diffuse mode, the potential drop is about 3 V.

3.4. Effects due to the presence of metal vapour

Metal atoms, in general, have many excited levels below the ionization potential of the shielding gas and are therefore more likely to be excited and ionized. The radiative emission and the electric conductivity of the plasma is therefore expected to increase in the presence of metal vapours. It is important to take into account the presence of metal vapours for a better understanding of TIG welding arcs. The influence of the metal vapour on the arc characteristics has been studied over the course of many years in experimental and modelling works arriving at contradictory results. On the one hand, the model of a free-burning arc
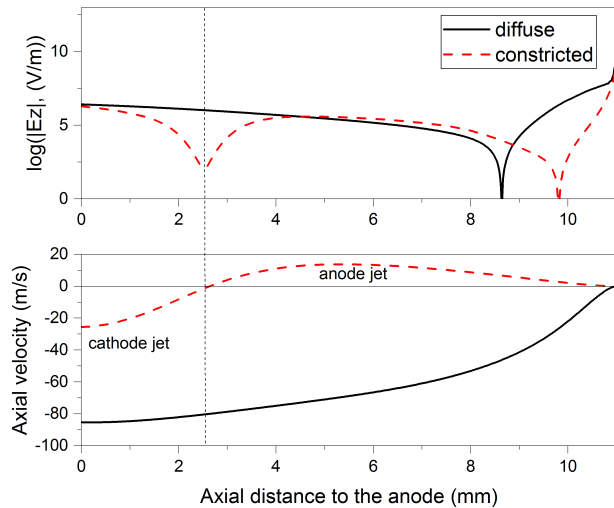
Figure 15. The flow velocity and the modulus of the electric field along the arc axis for the diffuse mode (solid line) and the constricted mode (dashed line) of arc attachment on the anode. Arc current 200 A.

by Gonzalez et al [33], which was based on the LTE assumption and assumed a temperature of 1000 K at the bottom surface of the anode, predicted a mass concentration of 9 % at the centre of the upper surface of the anode and 1 % at a distance of 10 mm from the anode surface for an arc current of 200 A and an inter-electrode distance of 10 mm. In this simulation, the temperature of the plasma column decreased significantly due to the increasing radiation losses. The effect led to a reduction of the heat flux to the anode and to a shrinking of the weld pool. On the other hand, the experimental studies in a free-burning arc with an inter-electrode distance of 5 mm and an arc current of 200 A by Farmer et al [34] showed a minor effect on the temperature in the presence of metal vapours released from the molten stainless-steel anode. Fe and Cr atoms were observed within a distance of 0.5 mm from the anode. More recent modelling results by Mougenot et al [35] at an arc current of 200 A showed a mass concentration of metal vapour of respectively 0.6 % at the anode centre and 0.1 % at a distance from the anode of 1 mm. Tanaka et al [36] studied an arc in argon at a current of 150 A and an inter-electrode distance of 5 mm and reported a maximum value of about 0.25 mol%. The models in [35, 36] are transient and developed respectively in 3D and 2D assuming LTE conditions. The main advance in these works was that flow in the molten weld pool was considered to provide a more realistic temperature at the upper anode surface. The temperature of the bottom anode surface was set at 300 K. A mass conservation equation is solved for the iron vapour and the viscosity approximation was used to express the diffusion coefficient.

The nonequilibrium model [19] has recently been extended to gas mixtures containing metal vapour. The general diffusion formulation includes atoms and singly charged ions of iron additionally to those of argon as the shielding gas. The concentration of iron vapour on the anode surface is used as a boundary condition. It is determined by the saturation vapour pressure (related to the temperature at the anode surface) and the ambient pressure [37]. The iron vapour pressure increases rapidly as the temperature at the anode surface approaches the boiling point of the material. The anode surface is assumed to be non-deformable and flat. A flow in the weld pool is not taken into account in the model at the current stage. The temperature at the bottom surface of the anode follows from the heat flux of unforced air cooling.

The two-dimensional distribution of the mass fraction of iron atoms and ions is shown respectively in Fig. 16 and Fig. 17 for an arc current of 150 A and an inter-electrode distance of 5 mm. The maximum mass fraction of Fe atoms and ions in the centre of the anode plate is about 0.6 %, which is close to the value reported in [35] at a higher arc current. The maximum temperature at the anode surface obtained with the nonequilibrium model is about 2050 K (Fig. 18). This value is lower than the value of 2200 K reported in [36] for an arc current of 150 A and that of 2310 K reported in [35] for an arc current of 200 A. The different results concerning the amount of metal vapours in [35, 36] can be probably explained by the different arc current values since both models consider the flow in the liquid weldpool and similar boundary conditions although the thermodynamic and transport properties applied in the models can differ. The main differences of the models [35, 36] to the nonequilibrium model is, however, the description of the arc plasma and the plasma-electrode interaction. Since no recirculations of the fluid flow can be seen in the region with iron atoms and ions (see the arrow indicators in Fig. 18), the peculiar structures shown in Figures 16 and 17 are the effects of species diffusion. The Fe atoms diffusing into the arc periphery are effectively ionized. At a distance of about 0.5 mm away from the anode surface, the mass fraction of Fe ions exceeds that of Fe atoms. The spatial distributions of Fe atoms and ions in the arc region point at off-axis maxima. The Fe atoms follow the fluid flow far away from the arc core towards the outlet, while the mass fraction Fe ions rapidly decreases. The appearance of an off-axis maximum in the distribution of Fe metal vapour was reported also in [35].

The results of the nonequilibrium model confirm the weak influence of iron metal vapours for a mass concentration up to 0.6 % and argon shielding gas reported in [35]. A stronger influence has been observed in helium arc plasma [36, 38] as the iron vapour has been found to increase the electrical conductivity at low temperatures. The decrease in the electron and heavy particle temperatures on the arc axis in the presence of iron vapours in comparison to the values in a pure argon plasma is almost negligible. Also, quite small is the increase in the voltage drop over the
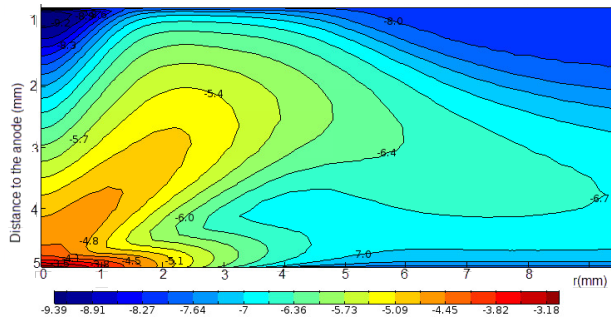
Figure 16. Mass fraction of iron atoms in the arc plasma at an arc current of 150 A and an inter-electrode distance of 5 mm. The presentation is in a logarithmic scale.
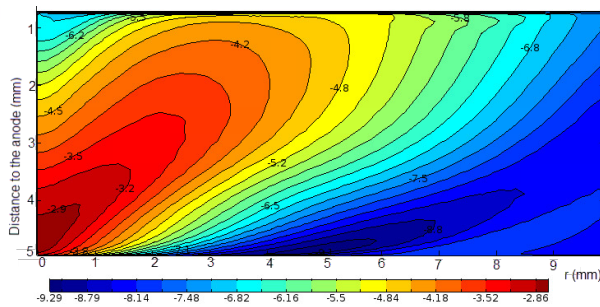

Figure 17. Mass fraction of iron ions in the arc plasma at an arc current of 150 A and an inter-electrode distance of 5 mm. The presentation is in logarithmic scale. The presentation is in a logarithmic scale.

arc column due to the increased radiative emission and the corresponding arc cooling.

Although the nonequilibrium model already significantly improves the description of the arc plasma and its interaction with the electrodes, further developments such as a proper treatment of the liquid metal phase, the deformation of the anode surface, and the motion of the arc relative to the anode are needed to extend its predictive capability to real welding applications. From a physical point of view, studies concerning the role of metastable states of the atoms of the shielding gas on the excitation of the metal ions will provide the answer whether the metal ions are in thermal equilibrium with the other heavy particles.

4. Conclusions

In this work, the state-of-the-art nonequilibrium modelling of DC tungsten-inert gas arcs is presented. One and the same physical model is applied to outline the effects of the cathode tip shape, the variation of the arc length, the formation of diffuse and constricted arc attachment modes on the anode, and the presence of metal vapour in atmospheric pressure argon arcs. The results are analyzed and discussed in relation to previously published experimental findings and modelling predictions.

It is shown that the arc plasma parameters strongly depend on the geometry of the cathode tip. The re-
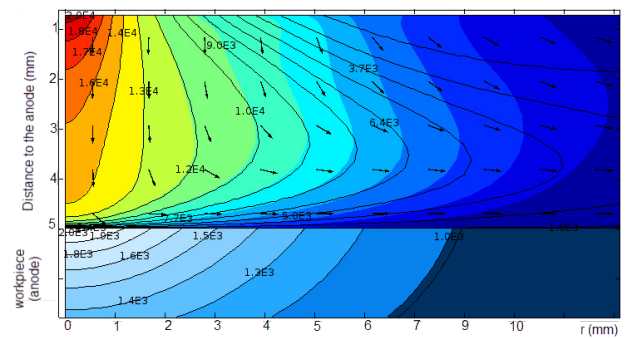

Figure 18. Temperature in kelvin of heavy particles (black lines) and electrons (filled coloured contours) in the arc region and in the workpiece. The flow field is presented by arrow indicators. Arc current 150 A, inter-electrode distance 5 mm.

sults obtained for a 60°-cathode and an arc current of 100 A show a weak dependence of the conditions near the cathode on the arc length in the range of inter-electrode distances 2–10 mm.

The formation of a constricted arc attachment on the anode is discussed in relation to the macroscopic flow conditions and the thermal and ionization nonequilibria occuring in the anode region.

For an anode made of iron, a maximum mass fraction of 0.6 % of iron atom and ions is predicted in the centre of the anode plate for an arc current of 150 A. The presence of metal vapour in this concentration causes a small decrease in the electron and heavy particle temperatures on the arc axis and a small decrease in the voltage drop over the arc column in comparison to the values in a pure argon plasma.

Acknowledgements

References

[1] A. B. Murphy. A perspective on arc welding research: The importance of the arc, unresolved questions and future directions. *Plasma Chemistry and Plasma Processing*, 35:471–489, 2015. doi:10.1007/s11090-015-9620-2

[2] J. J. Lowke and A. B. Murphy. Plasma flows. In R. W. Johnson, editor, *The handbook of fluid dynamics*, chapter 15. CRC Press, Boca Raton, 1998.

[3] M. S. Benilov. Understanding and modelling plasma-electrode interaction in high-pressure arc discharges: a review. *J. Phys. D: Appl. Phys.*, 41(14):144001 (30pp), 2008. doi:10.1088/0022-3727/41/14/144001

[4] J. Mentel and J. Heberlein. The anode region of low current arcs in high intensity discharge lamps. *J. Phys. D: Appl. Phys.*, 43:023002, 2010. doi:10.1088/0022-3727/43/2/023002

[5] N. A. Almeida, M. S. Benilov, and G. V. Naidis. Unified modelling of near-cathode plasma layers in high-pressure arc discharges. *J. Phys. D: Appl. Phys.*, 41:245201, 2008. doi:10.1088/0022-3727/41/24/245201

[6] I. L. Semenov, I. V. Krivtsun, and U. Reisgen. Numerical study of the anode boundary layer in atmospheric pressure arc discharges. *J. Phys. D: Appl. Phys.*, 49:105204, 2016. doi:10.1088/0022-3727/49/10/105204

[7] M. S. Benilov and M. Cunha. Heating of refractory cathodes by high-pressure arc plasmas I. *J. Phys. D: Appl. Phys.*, 35:1736–1750, 2002. doi:10.1088/0022-3727/35/14/314

[8] M. S. Benilov, M. Carpaij, and M. D. Cunha. 3D modelling of heating of thermionic cathodes by high-pressure arc plasmas. *J. Phys. D: Appl. Phys.*, 39:2124–2134, 2006. doi:10.1088/0022-3727/39/10/024

[9] F. Cayla, P. Freton, and J.-J. Gonzalez. Arc/cathode interaction model. *IEEE Transac. Plasma Sci.*, 36(4):1944–1953, 2008. doi:10.1109/TPS.2008.927378

[10] M. S. Benilov and A. Marotta. A model of the cathode region of atmospheric pressure arcs. *J. Phys. D: Appl. Phys.*, 28:1869–1882, 1995. doi:10.1088/0022-3727/28/9/015

[11] J. Wendelstorf. Ab initio modelling of thermal plasma gas discharges (electric acrs). Ph.D. Thesis, Univ. Braunschweig, Germany, 2000.

[12] J. J. Gonzalez et al. Two-dimensional self-consistent modelling of the arc/cathode interaction. *J. Phys. D: Appl. Phys.*, 42:145204, 2009. doi:10.1088/0022-3727/42/14/145204

[13] S. Gorchakov et al. Nonequilibrium arc model for the description of arc-electrode interaction. *Proceedings 27th ICEC*, 22-26 June Dresden, Germany, VDE Verlag, 2014.

[14] J. Shirvan and I. Choquet. Gtaw process - a review of cathode plasma coupling modelling. *Welding in the World*, 60:821835, 2016.

[15] M. Baeva. Thermal and chemical nonequilibrium effects in free-burning arcs. *Plasma Chemistry and Plasma Processing*, 36:151–167, 2016. doi:10.1007/s11090-015-9650-9

[16] J. Wendelstorf. Two-temperature, two-dimensional modelling of cathode-plasma interaction in electric arcs. *Proceedings 24th ICPIG*, 11-16 July Warsaw, Poland, v. 2 p. 227, 1999.

[17] H.-P. Li and M. S. Benilov. Effect of a near-cathode sheath on heat transfer in high-pressure arc plasmas. *J. Phys. D: Appl. Phys.*, 40:2010–2017, 2007. doi:10.1088/0022-3727/40/7/024

[18] M. Baeva et al. Two-temperature chemically non-equilibrium modelling of transferred arcs. *Plasma Sources Sci. Technol.*, 21:055027, 2012. doi:10.1088/0963-0252/21/5/055027

[19] M. Baeva et al. Novel non-equilibrium modelling of a DC electric arc in argon. *J. Phys. D: Appl. Phys.*, 49:245205, 2016. doi:10.1088/0022-3727/49/24/245205

[20] V. M. Zhdanov. *Transport phenomena in multicomponent plasma*. London: Taylor and Francis, 2002.

[21] J. D. Ramshaw. Self-consistent effective binary diffusion in multicomponent gas mixtures. *J. Non-Equilib. Thermodyn.*, 15:295–300, 1990. doi:10.1515/jnet.1990.15.3.295

[22] V. Rat et al. Treatment of non-equilibrium phenomena in thermal plasma flows. *J. Phys. D: Appl. Phys.*, 41:183001, 2008. doi:10.1088/0022-3727/41/18/183001

[23] M. S. Benilov et al. Account of near-cathode sheath in numerical models of high-pressure arc discharges. *J. Phys. D: Appl. Phys.*, 49:215201, 2016. doi:10.1088/0022-3727/49/21/215201

[24] COMSOL Multiphysics v.5.2a (Stockholm: COMSOL) http://www.comsol.com

[25] J. Haidar and A. J. D. Farmer. Large effects of cathode shape on plasma temperature in high-current free-burning arcs. *J. Phys. D: Appl. Phys.*, 27:555–560, 1994. doi:10.1088/0022-3727/27/3/019

[26] M. Baeva, E. Siewert, and D. Uhrlandt. Electric field and voltage of tig arcs from non-equilibrium modeling and experiment. *Proceedings Gas Discharges and Their Applications*, 11-16 September Nagoya, Japan, vol. 1, pp. 73-76, 2016.

[27] M. S. Benilov. Theory of nonlinear surface heating. *Phys. Scripta*, T84:22–46, 2000. doi:10.1238/Physica.Topical.084a00022

[28] M. Baeva. Non-equilibrium modeling of tungsten-inert gas arcs. *Plasma Chem. Plasma Process.*, 37:341–370, 2017. doi:10.1007/s11090-017-9785-y

[29] J. Heberlein, J. Mentel, and E. Pfender. The anode region of electric arcs: a survey. *J. Phys. D: Appl. Phys.*, 43:023001, 2010. doi:10.1088/0022-3727/43/2/023001

[30] R. V. Hartmann and J. V. Heberlein. Quantitative investigations on arc-anode attachments in transferred arcs. *J. Phys. D: Appl. Phys.*, 34:2972–2978, 2001. doi:10.1088/0022-3727/34/19/307

[31] T. Amakawa et al. Anode-boundary-layer behaviour in a transferred, high-intensity arc. *J. Phys. D: Appl. Phys.*, 31:2826–2834, 1998. doi:10.1088/0022-3727/31/20/017

[32] M. Baeva. A survey of chemical nonequilibrium in argon arc plasma. *Plasma Chem. Plasma Process.*, 37:513–530, 2017. doi:10.1007/s11090-016-9778-2

[33] J.-J. Gonzalez et al. Mathematical modeling of a free-burning arc in the presence of metal vapor. *J. Appl. Phys.*, 74(5):3065–3070, 1993. doi:10.1063/1.354624

[34] A. J. D. Farmer, G. N. Haddad, and L. E. Cram. Temperature determinations in a free-burning arc: III. measurements with molten anodes. *J. Phys. D: Appl. Phys.*, 19:1723–1730, 1986. doi:10.1088/0022-3727/19/9/016

[35] J. Mougenot et al. Plasma-weld pool interaction in tungsten-inert gas configuration. *J. Phys. D: Appl. Phys.*, 46:135206, 2013. doi:10.1088/0022-3727/46/13/135206

[36] M. Tanaka et al. Time-dependent calculations of molten pool formation and thermal plasma with metal vapour in gas tungsten arc welding. *J. Phys. D: Appl. Phys.*, 43:434009, 2010. doi:10.1088/0022-3727/43/43/434009

[37] G. Lago et al. A numerical modelling of an electric arc and its interaction with the anode: Part i. the two-dimensional model. *J. Phys. D: Appl. Phys.*, 37:883–897, 2004. doi:10.1088/0022-3727/37/6/013

[38] A. B. Murphy et al. Modelling of thermal plasmas for arc welding: the role of the shielding gas properties and of metal vapour. *J. Phys. D: Appl. Phys.*, 42:194006, 2009. doi:10.1088/0022-3727/42/19/194006